Duty Cycling of Waterjet Can Improve Steerability and Radius-of-Curvature (ROC) for Waterjet Steerable Needles

Mahdieh Babaiasl[1], Fan Yang[2], and John P. Swensen[3]

Abstract— **Steerable needles are a type of medical devices that can steer around obstacles to reach to a target location and thus can improve the accuracy of medical procedures. Radius-of-Curvature (ROC) is of paramount importance while designing steerable needles and achieving smaller radius and being able to control it is very important in evaluating the efficacy of the steerable needles. In this paper, the idea of a new class of steerable needle technology namely fracture-directed waterjet steerable needles is presented in which the direction of the tissue fracture is controlled by waterjet and then Nitinol tube follows. Needle steering tests are performed on two different stiffnesses of SEBS soft tissue simulants, as well as 10% by weight Knox Gelatin (Kraft Foods Global Inc., IL) as substitutes to real biological tissues. Curvature of the needle is controlled by waterjet duty cycling and it is shown that it can be controlled from about 0 (when waterjet is OFF at all steps) to maximum curvature (when waterjet is ON for all steps). It is concluded that the curvature is a linear function of the duty cycling and that the smallest ROC of the waterjet steerable needle (when waterjet is ON at all steps) is improved in comparison to the smallest ROC of traditional steerable needles in the same tissue phantom.**

I. INTRODUCTION

Steerable needles technology is relatively a new endeavor by several research groups around the world that is developed with the promise of improving the efficacy of medical procedures and biopsies [1], [2], [3], [4], [5]. Steerable needles came into existence to correct unwanted needle bending, and tissue motion in addition to steering around obstacles to avoid anatomical constraints, and reach to targets in the anatomy with greater accuracy [6], [7].

There are several steering techniques developed in the literature that an extensive review is provided in [8]. These techniques include base manipulation [9], bevel tip with and without curve [10], [11], precurved stylet [12], and active cannula [13], [14] among others. Among these methods, Flexure-Based Steerable Needles achieved the best radius-of-curvature to date [15]. These methods mostly rely on creating an asymmetric force at the tip of the needle to change the direction of the tissue fracture as the needle is inserted [16], [15]. Furthermore, these methods rely on the complex elastic interaction between the tip of the needle and the surrounding tissue to achieve an angled fracture direction. A complete discussion on the current limitations of the steerable needles is provided in [17]. Therefore, introducing new methods for needle steering that promise smaller ROC is necessary.

In traditional steerable needles, rotational duty cycling (periods of continual spinning) is used to adjust the curvature [15], [18], [19], [20]. However, rotational duty-cycle methods must account for the inherent torsional windup associated with twisting a long, super-elastic needle about the insertion axis[21], [22]. Therefore, introducing new and more efficient ways to adjust the radius of curvature in steerable needles seems to be lacking too.

In this paper, a new class of steerable needles namely fracture-directed waterjet steerable needles is used to achieve a significantly greater control over the direction of the tissue fracture. In waterjet needle steering, first the direction of the tissue is controlled by waterjet with sub-millimeter diameter, and then the flexible tube made of Nitinol follows the fractured path. The depth of the tissue fracture is controlled by adjusting the volumetric flow rate of the pump since our previous research [23] showed that considering all other variables constant, the depth-of-cut of waterjet in soft tissue is a linear function of the waterjet velocity exiting the needle. Furthermore, the angle of the tissue fracture is achieved using a fixed-angle nozzle that shoots the waterjet in an angle relative to the needle tip. Although this is one possible way of implementing fracture-directed steerable needles, this promises the potential of radius of curvature and steerablility that are unattainable with current tip steerable needles. Duty cycling of waterjet is used to control the curvature of the waterjet needle from approximately 0 (insertion without waterjet) to maximum curvature (insertion with waterjet ON for all steps), and it is shown that the curvature of the needle is a linear function of the duty cycling. The minimum radius of curvature achieved with this method in 10% by Weight Knox Gelatin soft tissue simulants is compared to the best ROCs obtained in the steerable needles literature in the same medium. It is shown that waterjet steerable needles can reach a smaller ROC in comparison to the conventional steerable needles in the same soft tissue simulants.

Fig. 1 shows the underlying principle of the waterjet steerable needles, in which the direction of the tissue fracture is controlled by angled waterjet and then the flexible Nitinol tube follows. This process continues until the waterjet needle reaches to a target location avoiding obstacles. The direction of the needle curvature can be changed by rotating the needle at the base. This photo shows the general form of the waterjet steerable needles in which the the nozzle angle can be controlled, however in the experiments in this paper,

[1]Mahdieh Babaiasl is a graduate research assistant with the School of Mechanical and Materials Engineering, Washington State University, Pullman, Washington, USA. mahdieh.babaiasl@wsu.edu

[2]Fan Yang is a graduate research assistant with the School of Mechanical and Materials Engineering, Washington State University, Pullman, Washington, USA. fan.yang6@wsu.edu

[5]John P. Swensen is an assistant professor with the School of Mechanical and Materials Engineering, Washington State University, Pullman, Washington, USA. john.swensen@wsu.edu

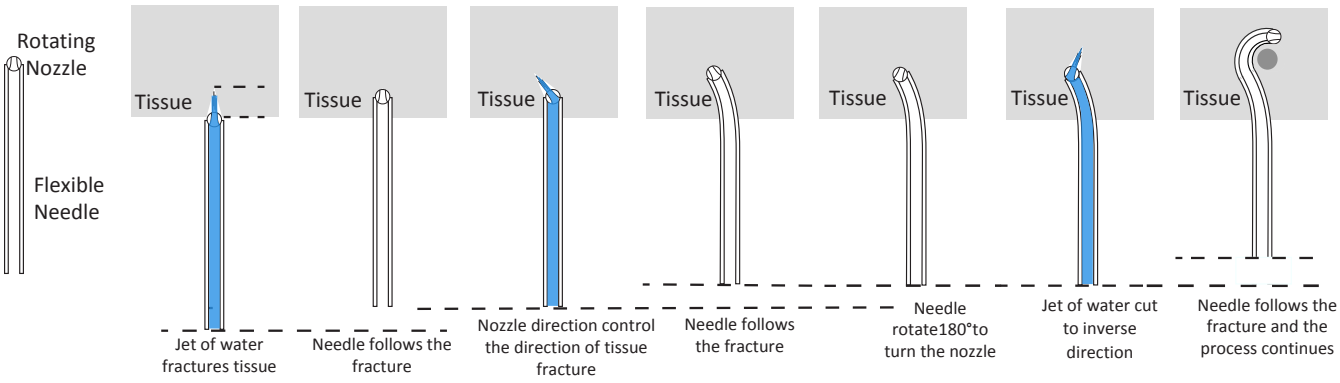

Fig. 1: Underlying Principle of Waterjet Steerable Needles. First, the direction of the tissue fracture is controlled by angled sub-millimeter waterjet, and then the flexible Nitinol tube follows the cut path. This process continuous till the needle avoids the obstacles and reaches to a target location. Direction of the curvature can be changed by rotating the base of the needle. Note that this figure shows the general principle of waterjet needle steering and the experiments in this paper are conducted using a fixed-angle nozzle shown in Fig. 2.

a fixed angle nozzle shown in Fig. 2 is used.

II. MATERIALS AND METHODS

A. Soft Tissue Phantoms Preparation

Poly (styrene-b-ethylene-co-butylene-b-styrene) triblock copolymer (SEBS) by Kraton Polymers LLC (G1650, Houston, TX, USA) is used as the main material for tissue-mimicking simulants of the first set of experiments. The solvent used for SEBS is light mineral oil, which makes it a more environmentally stable substitute for water-based hydrogels [24], [23], [5]. A complete procedure for making tissue mimicking simulants and tissue mechanical properties are available in our other publications. The interested reader may refer to [25], [23] for more information.

10% by Weight Knox Gelatin (Kraft Foods Global Inc., IL) soft tissue simulants is also used as the main tissue substitutes in experiments to compare the waterjet needle with traditional steerable needles since 10% by weight Knox Gelatin is the common tissue used in the literature for experiments with traditional steerable needles. Knox Gelatin is mixed with hot water until completely dissolved. Then the mixture is put in the vacuum chamber so that all the air bubbles trapped in the solution are disappeared. The solution is then poured into molds of $10 \times 10 \times 30$ mm and then put in the refrigerator at 4^o C for 8 hours before removing from the molds. Because of the water-based nature of the samples, and to avoid the samples from drying, all the experiments are done in the same day.

B. Experimental Setup and Waterjet Steerable Needle Design

Fig. 3 shows the experimental setup in which a high pressure pump (PR-class Dual Piston, PR100PFT3D, Scientific Systems Inc., State College, PA, USA) provides a computer-controlled volumetric flow rate (up to $100\frac{mL}{min}$). When the water velocity exceeds the threshold necessary to fracture the tissue, a channel will be cut at 38° relative to tangent to the needle tip, due to the nozzle design. Suction canister

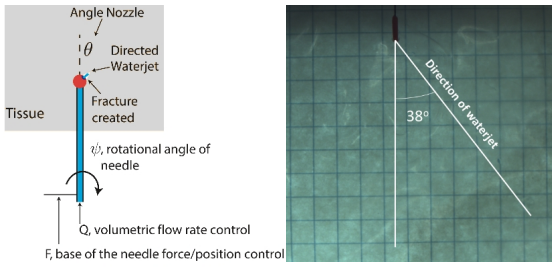

Fig. 2: Waterjet fixed-angle tip used in the experiments in this paper. (Left) Schematic of the fixed-angle nozzle principle, and (Right) Waterjet needle tip with 38^o angle used in this paper.

and a vacuum pump, are used to collect the water that sprays back out along the shaft of the needle during experiments. Telescopic sheath made of two concentric copper tubes is used to prevent buckling of the needle during insertions without waterjet (buckling is not an issue when inserting with waterjet). Rotation motor and gear are used to rotate the needle to change the direction of the steering.

The insertion unit consists of two components, a nickel-titanium tube (GoodFellow Corporation, Coraopolis, PA) and a 3D-printed polycaprolactone (PCL) nozzle. The nickel-titanium tube has 0.33mm outer diameter with 0.24mm inner diameter, and the PCL nozzle has 0.24mm inner diameter at the tip and 0.33 mm diameter at the base. The PCL nozzle was 3D-printed by FDM printer then attached to the nickel-titanium tube using cyanocrylate glue. Fig. 2-Left shows the schematic of the fixed-angle nozzle and Fig. 2-Right depicts the angle at which the designed needle cuts the tissue.

C. Waterjet Needle Steering Tests with Duty Cycling

In order to control the radius of curvature of the needle, duty cycling of waterjet is used. Fig. 4 shows the concept of duty cycling of waterjet to control the radius of curvature. 0% duty cycling means that waterjet is turned off for the

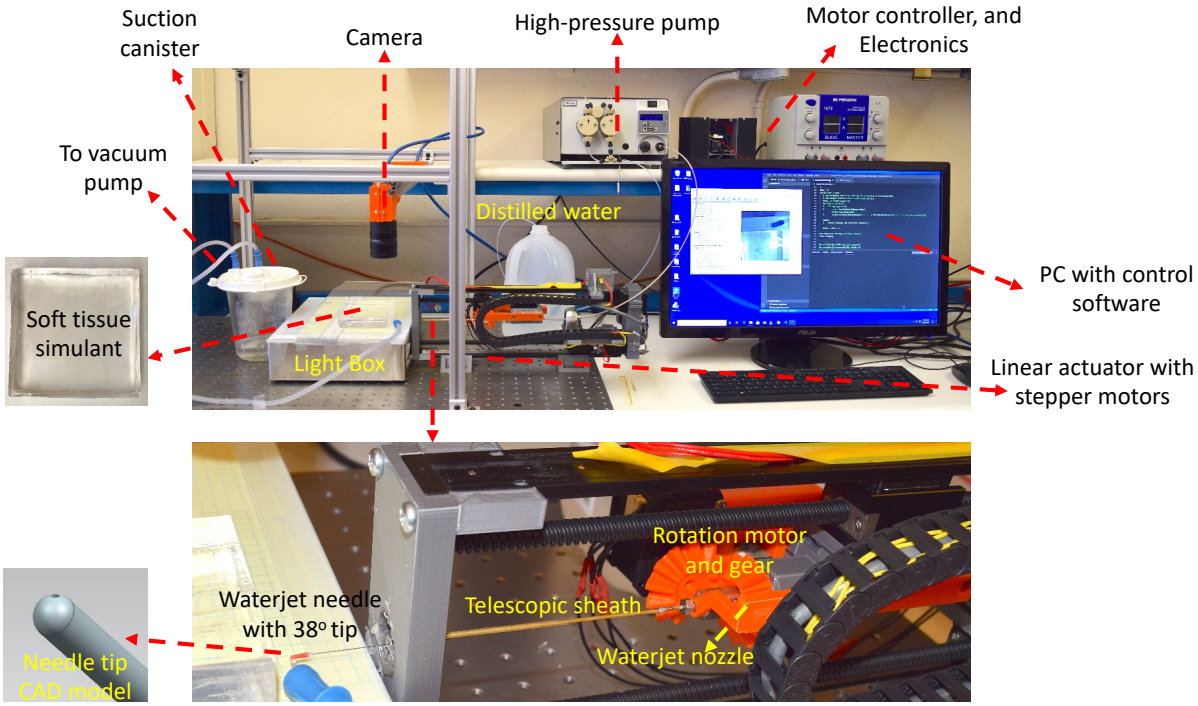

Fig. 3: Setup for waterjet needle steering tests. First, high-pressure pump is set to the desired flow rate based on the stiffness of the tissue (for 10% SEBS, 15% SEBS, and Knox Gelatin, the flow rates are set to 40, 70, and 10 $\frac{mL}{min}$), and then waterjet cuts a channel in tissue at 38° angle. The pump is turned off, and then the needle follows the channel with the velocity of insertion of 1 $\frac{mm}{s}$. For insertions without waterjet, the pump is turned off and the needle is inserted with velocity of insertion of 0.5 $\frac{mm}{s}$. Telescopic sheath made of two copper tubes is used to prevent buckling of the needle during insertions without waterjet. The needle has inner diameter (ID) of 0.24 mm, and outer diameter (OD) of 0.33 mm, and the tip has ID = 0.24 mm.

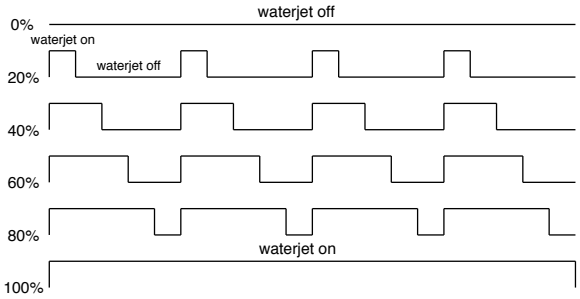

Fig. 4: Schematic of duty cycling of waterjet in order to control the radius of curvature of the needle. For 0% duty cycling, the waterjet is off through the length of insertion and needle is inserted without waterjet, and 100% duty cycling means that waterjet is ON for the entire length of insertion.

entire length of insertion, and 100% duty cycling means that waterjet is ON in the whole length of insertion. 3 tests are performed for each duty cycling rate and the average radius of curvature and standard deviation are calculated.

D. Measurement of Radius-of-Curvature

Radius-of-curvature of the needle during duty cycling experiments is measured using a custom-developed software in Matlab that first imports the photo and calibrates the axes based on the rulers of the photo and then fits a curve to the needle path to find the radius of curvature of the needle.

III. Results

In this section, results of duty cycling of waterjet in order to control the curvature of the needle are presented in SEBS and Knox Gelatin soft tissue simulants. The smallest ROC in Knox Gelatin tissues is compared to the best ROC for conventional steerable needles in literature conducted in the same tissue environment.

A. Duty Cycling of Waterjet for Waterjet Steerable Needles Can Improve Steerablity and Radius-of-Curvature

Fig. 5-Left, and Middle show the results of radius of curvature control using duty cycling of waterjet in 10% (Tissue A), and 15% (Tissue B) SEBS in mineral oil soft tissue simulants. Fig. 5-Right shows the insertion of the needle with no tip while the waterjet cuts a straight channel in the tissue and then the needle follows the channel. Fig. 6-UP(Left) represents the results of radius of curvature control using duty cycling of waterjet in 10% by Weight Knox Gelatin soft tissue simulants (Tissue C). As can be seen from these figures, duty cycling of waterjet can be used to control the curvature of the needle from almost 0 (insertion without waterjet) to maximum curvature (insertion with waterjet ON

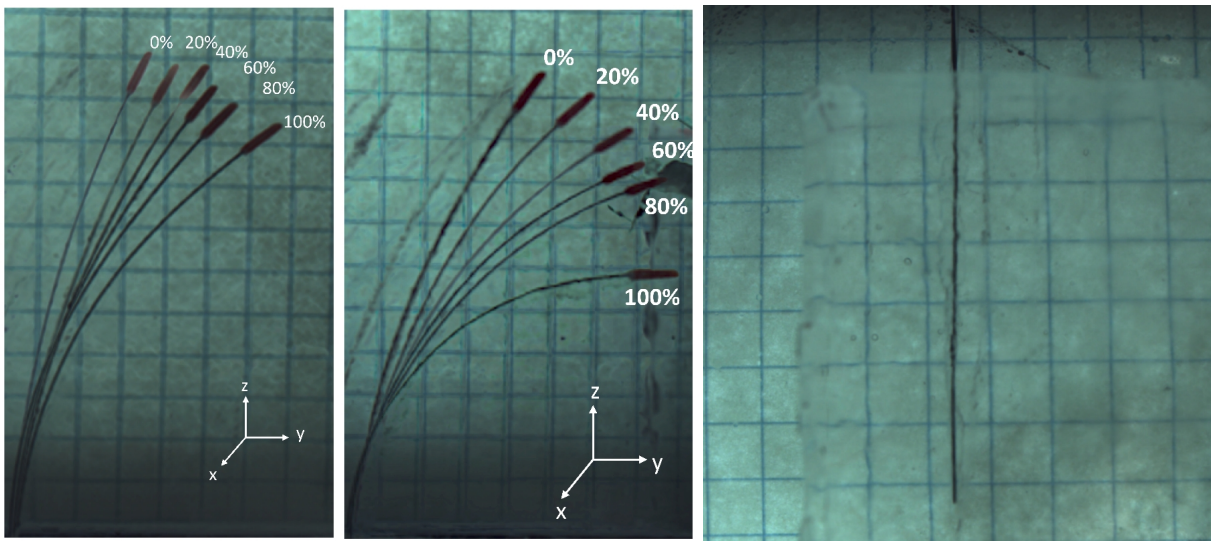

Fig. 5: Waterjet duty cycling to control the radius of curvature of the waterjet steerable needle. (Left) 10% SEBS in mineral oil soft tissue simulants (Tissue A), and (Middle) 15% SEBS in mineral oil soft tissue simulants (Tissue B). The figures are obtained by overlaying 6 different experiments. The total insertion length is 70 mm. Flow rates of $40\frac{ml}{min}$, and $70\frac{ml}{min}$ are used to get the same cut-depths in the same amount of time for Tissue A, and Tissue B, respectively. The best ROC for Tissue A, and Tissue B are 75, and 49 mm. (Right) obtaining straight insertion using waterjet needle with no tip. The needle follows the cut path by waterjet.

for all steps). For Tissue A, and Tissue B, volumetric flow rates of $40\frac{ml}{min}$, and $70\frac{ml}{min}$ are used, respectively (these flow rates give the same depth of cut in a given time in both tissues). For Tissue C, volumetric flow rate of $10\frac{ml}{min}$ is used to cause the same cut-depth in each step. Fig. 6-UP(Right) shows the Bicycle model [26], [27] of the needle motion, and Fig. 6-Bottom depicts the overlay of the Bicycle model with needle path. As it is evident, there is a high agreement between the experiments and the model.

Table I presents a comparison of the Smallest Radius of Curvature obtained with Waterjet Steerable needle and two of the conventional steerable needles in literature in the same soft tissue medium. Flexture-based steerable needles are known to have the smallest radius of curvature in the literature [15].

B. Curvature of the needle is a Linear Function of Waterjet Duty Cycling in a Range of Tissue Stiffnesses

Fig. 7, and 8 depict the Curvature (cm^{-1}) vs., duty cycling for Tissues A, B, and C, respectively. Curvature is calculated by averaging the 3 trials, and the error bars are one standard deviation above and one standard deviation below the data points. As can be seen from these figures, curvature of waterjet steerable needle is a linear function of duty cycling of waterjet for the range of tissue stiffnesses tested in this paper. Curvature (κ) can be easily calculated by inverting the radius of curvature:

$$\kappa = \frac{1}{r} \tag{1}$$

IV. DISCUSSION

In this paper, duty cycling of waterjet is used to control the curvature of the waterjet steerable needles. The results showed that duty cycling of waterjet can lead to Radii of curvature as low as 75, 49, and 78 mm in soft tissue phantoms made of 10% SEBS in mineral oil (Tissue A), 15% SEBS in mineral oil (Tissue B), and 10% by weight Knox Gelatin (Tissue C), respectively. The results are compared to the traditional steerable needles, and it is shown that waterjet steerable needle can reach to a ROC of 78 mm in Tissue C, where as the Bevel tip and Flexture-based needles reach to 178, and 121 mm in the same medium.

In Fig. 5, the needle curves in SEBS soft tissue simulants even when duty cycling is at 0%, whereas this is not the case in Fig. 6 for Tissue C. The reason for this is that the stiffnesses of Tissue A, and Tissue B are higher than Tissue C and the tiny bevel angle of the tip of the waterjet steerable needle interacts with Tissues A, and B causing it to bend. Fan et al. [5] showed that the curvature of the needle is a function of bending stiffness of the tissue and the needle and in the case of Tissue C, the bending stiffness is lower in comparison to the Tissue A, and B. On the other hand, the needle used in our study has a sub-millimeter tip (0.24 mm) which is much thinner and more flexible in comparison to the needles used in the literature therefore having a low bending stiffness. The combined effect of the low bending stiffness of the needle and high bending stiffness of the Tissues A, and B lead to bending of the needle even when the duty cycling is at 0%. This issue can be solved by manufacturing better tips without this tiny bevel effect. In the current research, we are using heat shrinkable material to manufacture reproducible

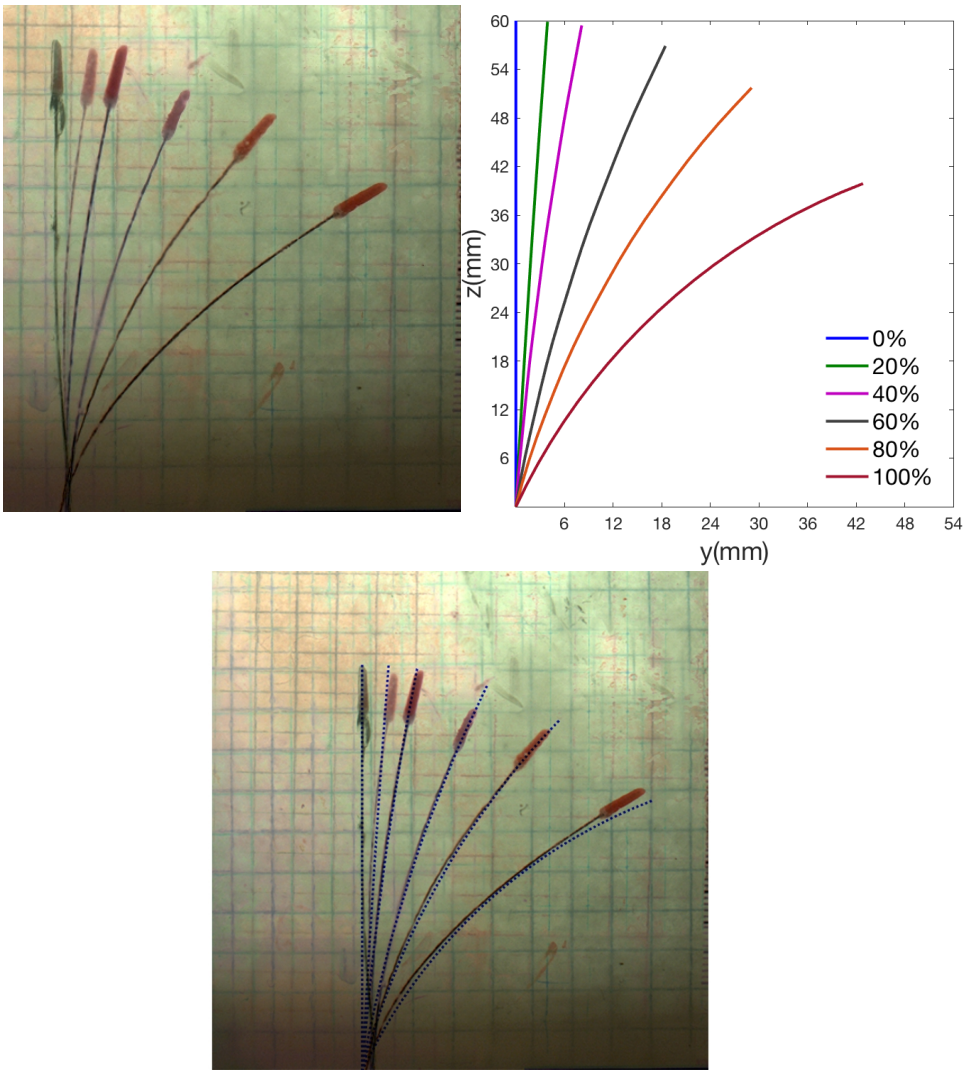

Fig. 6: UP(Left) Controlling the curvature of the needle in 10% by weight Knox Gelatin soft tissue phantoms (Tissue C) by duty cycling of the waterjet. The total insertion length is 60 mm. Flow rate of $10\frac{ml}{min}$ is used to get the depth of cut of 3mm in each insertion step. UP(Right) Bicycle model of the needle motion, and (Bottom) Overlay of the needle path with model.

TABLE I: Comparison of Smallest Radius of Curvature (ROC) of Waterjet Steerable Needle with Conventional Steerable Needles in the Same Medium.

Reference	Waterjet Steerable Needle	[28]	[15]
Needle Design/Material	Custom-designed/Nitinol Tube	Bevel tip/Rubber-like	Bevel tip with flexture/Stainless steel and Nitinol
Outer Diameter (mm)	0.33	12	0.91
Smallest ROC (mm)	78	178	121
Insertion Speed (mm/s)	1	1	5
Soft Tissue	Gelatin 10%	Gelatin 6%	Gelatin 10%

tips that are symmetrical with no tiny bevel angle to address this issue.

Insertion velocity of $1\frac{mm}{s}$ is chosen to insert the needle in the fractured path. This insertion velocity is known to be relevant to insertions in real medical applications [29]. Flow rates are set to 40, 70, and 10 $\frac{mL}{min}$) for Tissues A, B, and C, respectively. Experimental results showed that these flow rates cause the same depth of fracture of 3 mm in these soft tissues in a given time thus keeping the step lengths the same throughout the experiments.

In this paper nozzle with fixed angle of 38^o is used to cause angled fracture in tissue. Understanding the relationship between fixed angle nozzle and minimum achievable radius of curvature is important. It seems that minimum radius of curvature will be improved with increased nozzle angle. However, there might be some critical angle near

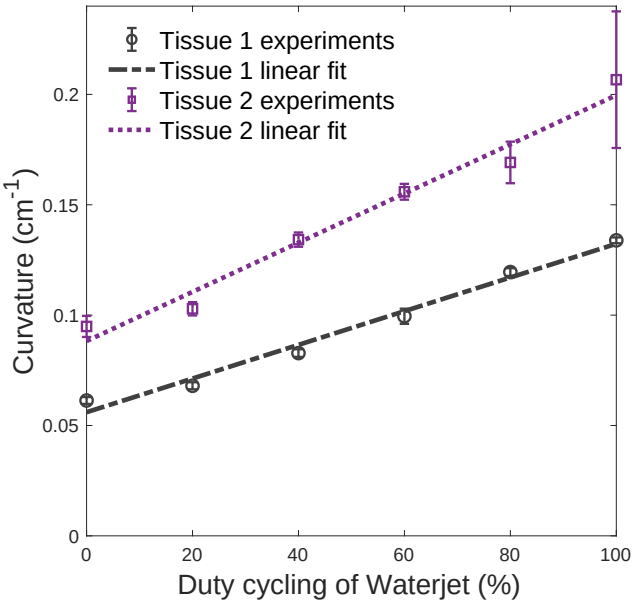

Fig. 7: Curvature of waterjet steerable needle vs. duty cycling of waterjet for two different tissue stiffnesses. The values reported for Curvature are the average of the 3 trials. The error bars are one standard deviation above and one standard deviation below the data points. For Tissue A, the goodness of the fit is $R^2 = 0.9839$, and for Tissue B, $R^2 = 0.98$.

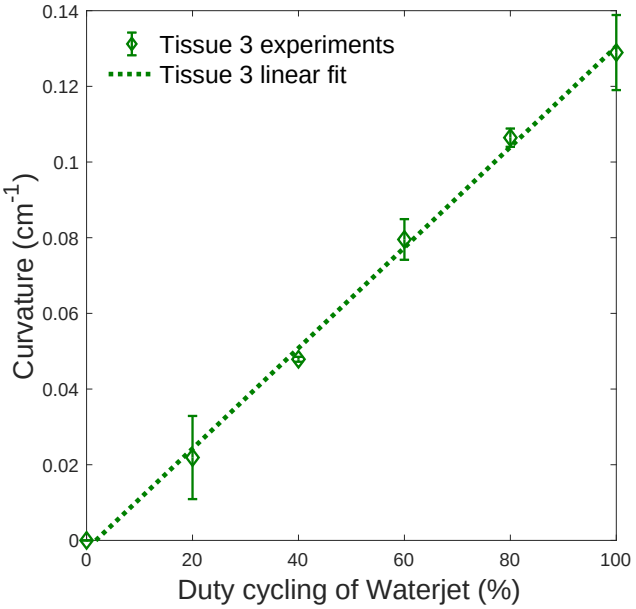

Fig. 8: Curvature of waterjet steerable needle vs. duty cycling of waterjet in Tissue C. The values reported for Curvature are the average of the 3 trials. The error bars are one standard deviation above and one standard deviation below the data points. The goodness of the fit is $R^2 = 0.9973$.

90 degrees after which the minimum radius of curvature does not improve anymore. Therefore, it is also necessary to study the effect of the nozzle angle on achievable radius of curvature of the waterjet steerable needle.

Young's moduli of Tissues A, and B are 27, and 68, respectively, which are relevant to stiffnesses of real biological tissues [30]. In particular, they are similar to uterus, and cervix tissues, the Young's moduli of which are in the range of $30-90$ kPa [31], prostate in the range of $62-69$ kPa [32], thrombus in the range of $8-38$ kPa [33], breast with modulus of 29 kPa [34], and muscle in the range of $7-57$ kPa [35], [36]. Tissue C is also used because this tissue is widely used in literature as the main soft tissue phantom [15], [28]. This made it possible to compare the results of the waterjet steerable needle to conventional steerable needles.

Duty cycling of waterjet is used to control the curvature of the waterjet steerable needle. The reason that increasing duty cycling of waterjet improved the radius of curvature is that during the times that waterjet is ON, an angled path is cut in the tissue that causes the needle to curve in contrast to insertions with no waterjet that needle almost travels straight. Therefore, the radius of curvature is smaller for experiments where waterjet is ON during the steps and the more steps the waterjet is ON the smaller the radius.

Experimental results showed that the radius of curvature is smaller in stiffer tissues. Yang et al. [5] demonstrated that the curvature of the needle is a function of the bending stiffness of the needle as well as the bending stiffness of the tissue. For harder tissues, the bending stiffness of the tissue is larger thus making the needle to curve more while following the cut path by waterjet.

V. CONCLUSIONS AND FUTURE WORK

In this paper, a new class of steerable needles namely fracture-directed waterjet steerable needles is introduced. In waterjet steerable needles, the direction of the tissue fracture is controlled by waterjet and then the steerable needle follows. Because of the needle tip design which has a 38^o angle from horizontal, a path can be cut at an angle in the tissue that helps the needle to steer by following the path. It is shown that curvature of waterjet needle can be controlled by duty cycling of waterjet (that means the duration of the whole insertion that the waterjet is ON) from 0% to 100% rates, and the best radii of curvature can be obtained by 100% waterjet duty cycling which are 74 mm, 49 mm, and 78 mm for Tissues A, B, and C, respectively. It is found that curvature is a linear function of duty cycling for the range of tissue stiffnesses tested in this paper and that the best radius of curvature obtained by waterjet is improved in comparison to the conventional steerable needles.

This paper explores the results in soft tissue simulants, whereas the current research is on testing and steering the waterjet needle in *ex vivo* real biological tissues. The effect of fixed nozzle angle on radius of curvature will also be studied in the future.

ACKNOWLEDGMENT

The authors would like to thank Alex Rodrigues and Sean Journot for their help in the experimental setup as well as Kraton Polymers LLC to provide samples of Kraton G1650, and G1652 for research.

REFERENCES

[1] X. Hu, A. Chen, Y. Luo, C. Zhang, and E. Zhang, "Steerable catheters for minimally invasive surgery: a review and future directions," *Computer Assisted Surgery*, vol. 23, no. 1, pp. 21–41, 2018.

[2] P. Moreira, G. van de Steeg, T. Krabben, J. Zandman, E. E. Hekman, F. van der Heijden, R. Borra, and S. Misra, "The miriam robot: A novel robotic system for mr-guided needle insertion in the prostate," *Journal of medical robotics research*, vol. 2, no. 04, p. 1750006, 2017.

[3] P. J. Swaney, A. W. Mahoney, B. I. Hartley, A. A. Remirez, E. Lamers, R. H. Feins, R. Alterovitz, and R. J. Webster III, "Toward transoral peripheral lung access: Combining continuum robots and steerable needles," *Journal of medical robotics research*, vol. 2, no. 01, p. 1750001, 2017.

[4] M. Abayazid, P. Moreira, N. Shahriari, A. Zompas, and S. Misra, "Three-dimensional needle steering using automated breast volume scanner (abvs)," *Journal of medical robotics research*, vol. 1, no. 01, p. 1640005, 2016.

[5] F. Yang, M. Babaiasl, and J. P. Swensen, "Fracture-directed steerable needles," *Journal of Medical Robotics Research*, vol. 4, no. 01, p. 1842002, 2019.

[6] T. L. De Jong, N. J. van de Berg, L. Tas, A. Moelker, J. Dankelman, and J. J. van den Dobbelsteen, "Needle placement errors: do we need steerable needles in interventional radiology?" *Medical devices (Auckland, NZ)*, vol. 11, p. 259, 2018.

[7] N. J. Cowan, K. Goldberg, G. S. Chirikjian, G. Fichtinger, R. Alterovitz, K. B. Reed, V. Kallem, W. Park, S. Misra, and A. M. Okamura, "Robotic needle steering: Design, modeling, planning, and image guidance," in *Surgical robotics*. Springer, 2011, pp. 557–582.

[8] N. J. van de Berg, D. J. van Gerwen, J. Dankelman, and J. J. van den Dobbelsteen, "Design choices in needle steeringa review," *IEEE/ASME Transactions on Mechatronics*, vol. 20, no. 5, pp. 2172–2183, 2014.

[9] S. P. DiMaio and S. Salcudean, "Needle steering and model-based trajectory planning," in *International Conference on Medical Image Computing and Computer-Assisted Intervention*. Springer, 2003, pp. 33–40.

[10] R. J. Webster, J. Memisevic, and A. M. Okamura, "Design considerations for robotic needle steering," in *Proceedings of the 2005 IEEE International Conference on Robotics and Automation*. IEEE, 2005, pp. 3588–3594.

[11] R. Alterovitz, K. Goldberg, and A. Okamura, "Planning for steerable bevel-tip needle insertion through 2d soft tissue with obstacles," in *Proceedings of the 2005 IEEE international conference on robotics and automation*. IEEE, 2005, pp. 1640–1645.

[12] S. Okazawa, R. Ebrahimi, J. Chuang, S. E. Salcudean, and R. Rohling, "Hand-held steerable needle device," *IEEE/ASME Transactions on Mechatronics*, vol. 10, no. 3, pp. 285–296, 2005.

[13] P. Sears and P. Dupont, "A steerable needle technology using curved concentric tubes," in *2006 IEEE/RSJ international conference on intelligent robots and systems*. IEEE, 2006, pp. 2850–2856.

[14] R. J. Webster, A. M. Okamura, and N. J. Cowan, "Toward active cannulas: Miniature snake-like surgical robots," in *2006 IEEE/RSJ international conference on intelligent robots and systems*. IEEE, 2006, pp. 2857–2863.

[15] P. J. Swaney, J. Burgner, H. B. Gilbert, and R. J. Webster, "A flexure-based steerable needle: high curvature with reduced tissue damage," *IEEE Transactions on Biomedical Engineering*, vol. 60, no. 4, pp. 906–909, 2012.

[16] T. K. Adebar, J. D. Greer, P. F. Laeseke, G. L. Hwang, and A. M. Okamura, "Methods for improving the curvature of steerable needles in biological tissue," *IEEE Transactions on Biomedical Engineering*, vol. 63, no. 6, pp. 1167–1177, 2015.

[17] C. Rossa and M. Tavakoli, "Issues in closed-loop needle steering," *Control Engineering Practice*, vol. 62, pp. 55–69, 2017.

[18] M. Fu, A. Kuntz, R. J. Webster, and R. Alterovitz, "Safe motion planning for steerable needles using cost maps automatically extracted from pulmonary images," in *2018 IEEE/RSJ International Conference on Intelligent Robots and Systems (IROS)*. IEEE, 2018, pp. 4942–4949.

[19] D. S. Minhas, J. A. Engh, M. M. Fenske, and C. N. Riviere, "Modeling of needle steering via duty-cycled spinning," in *2007 29th Annual International Conference of the IEEE Engineering in Medicine and Biology Society*. IEEE, 2007, pp. 2756–2759.

[20] A. Majewicz, J. J. Siegel, A. A. Stanley, and A. M. Okamura, "Design and evaluation of duty-cycling steering algorithms for robotically-driven steerable needles," in *2014 IEEE International Conference on Robotics and Automation (ICRA)*. IEEE, 2014, pp. 5883–5888.

[21] K. B. Reed, A. M. Okamura, and N. J. Cowan, "Modeling and control of needles with torsional friction," *IEEE Trans. Biomed. Eng.*, vol. 56, no. 12, pp. 2905–2916, Dec. 2009, nIHMS192959. [Online]. Available: http://dx.doi.org/10.1109/TBME.2009.2029240

[22] J. P. Swensen and N. J. Cowan, "Torsional dynamics compensation enhances robotic control of tip-steerable needles," in *Robotics and Automation (ICRA), 2012 IEEE International Conference on*. IEEE, 2012, pp. 1601–1606.

[23] M. Babaiasl, F. Yang, Y. Chen, J.-L. Ding, and J. P. Swensen, "Predicting depth of cut of water-jet in soft tissue simulants based on finite element analysis with the application to fracture-directed water-jet steerable needles," in *2019 International Symposium on Medical Robotics (ISMR)*. IEEE, 2019, pp. 1–7.

[24] R. A. Mrozek, B. Leighliter, C. S. Gold, I. R. Beringer, H. Y. Jian, M. R. VanLandingham, P. Moy, M. H. Foster, and J. L. Lenhart, "The relationship between mechanical properties and ballistic penetration depth in a viscoelastic gel," *Journal of the mechanical behavior of biomedical materials*, vol. 44, pp. 109–120, 2015.

[25] M. Babaiasl, F. Yang, and J. P. Swensen, "Towards water-jet steerable needles," in *2018 7th IEEE International Conference on Biomedical Robotics and Biomechatronics (Biorob)*. IEEE, 2018, pp. 601–608.

[26] R. J. Webster III, J. S. Kim, N. J. Cowan, G. S. Chirikjian, and A. M. Okamura, "Nonholonomic modeling of needle steering," *The International Journal of Robotics Research*, vol. 25, no. 5-6, pp. 509–525, 2006.

[27] T. K. Adebar and A. M. Okamura, "Recursive estimation of needle pose for control of 3d-ultrasound-guided robotic needle steering," in *2014 IEEE/RSJ International Conference on Intelligent Robots and Systems*. IEEE, 2014, pp. 4303–4308.

[28] S. Y. Ko, L. Frasson, and F. R. y Baena, "Closed-loop planar motion control of a steerable probe with a programmable bevel inspired by nature," *IEEE Transactions on Robotics*, vol. 27, no. 5, pp. 970–983, 2011.

[29] N. Abolhassani, R. Patel, and M. Moallem, "Control of soft tissue deformation during robotic needle insertion," *Minimally invasive therapy & allied technologies*, vol. 15, no. 3, pp. 165–176, 2006.

[30] P. N. Wells and H.-D. Liang, "Medical ultrasound: imaging of soft tissue strain and elasticity," *Journal of the Royal Society Interface*, vol. 8, no. 64, pp. 1521–1549, 2011.

[31] M. Z. Kiss, M. A. Hobson, T. Varghese, J. Harter, M. A. Kliewer, E. M. Hartenbach, and J. A. Zagzebski, "Frequency-dependent complex modulus of the uterus: preliminary results," *Physics in Medicine & Biology*, vol. 51, no. 15, p. 3683, 2006.

[32] T. A. Krouskop, T. M. Wheeler, F. Kallel, B. S. Garra, and T. Hall, "Elastic moduli of breast and prostate tissues under compression," *Ultrasonic imaging*, vol. 20, no. 4, pp. 260–274, 1998.

[33] H. Xie, K. Kim, S. R. Aglyamov, S. Y. Emelianov, M. ODonnell, W. F. Weitzel, S. K. Wrobleski, D. D. Myers, T. W. Wakefield, and J. M. Rubin, "Correspondence of ultrasound elasticity imaging to direct mechanical measurement in aging dvt in rats," *Ultrasound in Medicine and Biology*, vol. 31, no. 10, pp. 1351–1359, 2005.

[34] L. Han, J. A. Noble, and M. Burcher, "A novel ultrasound indentation system for measuring biomechanical properties of in vivo soft tissue," *Ultrasound in Medicine and Biology*, vol. 29, no. 6, pp. 813–823, 2003.

[35] K. Parker, S. Huang, R. Musulin, and R. Lerner, "Tissue response to mechanical vibrations for sonoelasticity imaging," *Ultrasound in Medicine and Biology*, vol. 16, no. 3, pp. 241–246, 1990.

[36] S. F. Levinson, M. Shinagawa, and T. Sato, "Sonoelastic determination of human skeletal muscle elasticity," *Journal of biomechanics*, vol. 28, no. 10, pp. 1145–1154, 1995.